Recent Advances in Helical Piles for Dynamic and Seismic Applications

M. Hesham El Naggar

Western University, London ON N6A 5B9, Canada
naggar@uwo.ca

Abstract. Helical piles have become popular foundation option owing to their many advantages related to ease of installation and large load carrying capacity. They are typically manufactured of straight steel shafts fitted with one or more helices and are installed using mechanical torque. They can sustain static and dynamic loading and are increasingly used in applications that induce complex loading conditions on them. The behavior and design of single vertical helical piles subjected to static loading is well investigated. However, a few studies investigated the dynamic or seismic behavior of single helical piles and their group behavior. This paper presents recent advances in evaluating the axial and lateral capacity and performance of helical piles and their response to dynamic and seismic loads.

Keywords: helical pile, dynamic response, seismic response, field tests.

1 Introduction

A helical pile (HP) consists of a central shaft with one or more pitched helical bearing plates affixed to it. It is typically manufactured of straight steel shaft fitted with one or more helices and is installed using mechanical torque. It could be installed to varying depths and at varying angle to suit the project needs and the available soil conditions. Helical piles are gaining wide popularity and are currently considered a preferred foundation option in a wide range of engineering projects to provide high compressive, uplift, and lateral resistance to static and dynamic loads. They are used to support buildings, bridges, telecommunication towers, power transmission lines and wind turbines (Elsharnouby and El Naggar, 2012a&b; Elkasabgy and El Naggar, 2013& 2015). More recently, they have become a preferred option in projects involving machine foundations and pipeline supports (Elkasabgy and El Naggar, 2018). These applications involve various loading conditions ranging from the typical primarily compressive loading with minimal lateral loading, to more complex loading conditions with significant lateral loading and rocking moment accompanied by small compressive loading (Fahmy and El Naggar, 2016a&b; Elkasabgy and El Naggar, 2019). It is necessary to have clear understanding of helical piles performance characteristics to ensure efficient and reliable design under these complex loading conditions.

Recent case histories proved that HPs exhibited outstanding performance during earthquakes (Elsawy et al. 2019). In addition, Fayez et al. (2021a&b) investigated the seismic response of HP groups in dry, dense sand deposits through full-scale shaking table tests. They reported that the pile group's lateral resistance comprised a flexural component and a rocking component, which was derived from the individual piles' axial resistance and was enhanced by the contribution of the helices. Orang et al. (2021) further studied the seismic response of HPs in liquefiable soil as a strategy to minimize the settlement of the shallow foundation employing large shaking table tests. Their results indicated that the HPs could reduce the post-liquefaction settlement of the supported foundation. The studies reviewed above collectively indicate the advantageous performance of helical piles under complex, dynamic and seismic loads. This paper provides the current state of knowledge related to the dynamic and seismic performance of helical piles.

2 Axial Capacity of Helical Piles

The compressive capacity of the helical pile is provided by a combination of shaft resistance and bearing resistance on the helices, i.e.

$$Q_c = Q_f + Q_b \quad (1)$$

where: Q_c is the ultimate compressive capacity; Q_f is the friction resistance along the shaft; and Q_b is the bearing resistance on the helical plates. The relative contributions of shaft and bearing resistances depend on the embedment depth, the soil layering and the pile geometry (i.e. shaft diameter, d, and helix diameter, D_h).

The ultimate compressive capacity of helical piles is predicted employing limit equilibrium methods, i.e., the static equilibrium of the pile at onset of soil failure around the pile. For helical piles with multiple helices, there are two possible failure mechanisms: individual bearing (IB) failure (Fig. 1a); or cylindrical shear (CS) failure (Fig. 1b) (Livneh and El Naggar, 2008; Perko, 2009; and Elsherbiny and El Naggar, 2013). For helical piles installed in sand, the failure mechanism is primarily IB, while for piles installed in clay it depends on inter-helix spacing, S_r (CS for $S_r < 2D_h$; IB for $S_r > 3D_h$; and either for $2D_h < S_r < 3D_h$). Helix diameter is typically 2 to 3 times the shaft diameter: therefore, a helical pile with one helix would provide 4 to 9 times the bearing resistance of a conventional pile with same pile embedment, shaft diameter, and soil strength parameters. Consequently, the helical pile capacity is derived primarily from bearing resistance along helices, especially when they are placed within the strong layer(s) within the soil profile, or from a combination of shaft friction and end-bearing.

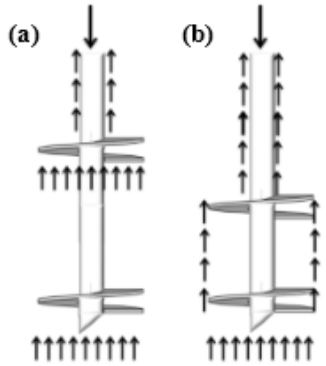

Fig. 1. Possible failure mechanisms of a multi-helix pile:
a) individual bearing failure; and b) cylindrical shear failure

The pile capacity considering IB failure mechanism is simply calculated as the sum of individual helix bearing capacities (i.e., each helical plate is considered as an individual plate bearing on soil beneath it). The pile capacity considering CS failure mechanism is calculated as the sum of frictional resistance along the inter-helical soil cylinder and the bearing on the bottom helix. Tappenden (2007) evaluated the performance of these methods based on the results of 29 full-scale axial load tests. Similarly, the field study results indicated that there was no distinct transition from CS to IB behavior for multi-helix anchors in clay (Lutenegger, 2009). Elsherbiny and El Naggar (2013) conducted a comprehensive study involving field testing and finite element modeling to evaluate the compressive capacity of helical piles installed in cohesive and cohesionless soil profiles. They reported that the predictions of theoretical equations for piles in cohesionless soil vary largely depending on the choice of bearing capacity factors and proper failure criteria. They also evaluated the interaction of closely spaced helices and proposed a bearing capacity reduction factor, R, and helix efficiency factor, E_H, to evaluate the compressive capacity of helical piles in cohesionless soil considering an industry acceptable ultimate load criterion corresponding to settlement equal to 5% of helix diameter, D_h, as discussed below.

2.1 Axial Capacity of Helical Piles in Sand

The axial capacity of helical piles installed in sand based on CS failure is given by:

$$Q_c = \gamma` H_2 A_2 N_q + \pi/2\, D_h \gamma` (H_2^2 - H_1^2) K_s \tan\phi + P_s/2\, H_{eff}^2\, \gamma` K_s \tan\delta \qquad (2)$$

where: Q_c = ultimate compression capacity; γ' = effective unit weight of soil; K_s = coefficient of lateral earth pressure for piles in compression; ϕ = the soil peak internal friction angle; A_2 = surface area of the bottom helix; N_q = bearing capacity factor $N_q = e^{\pi \tan\phi} \tan^2(45°+\phi/2)$; H_{eff} = the effective shaft length, shaft length above top helix –

helix diameter; H_1 = depth to top helix; H_2 = depth to bottom helix; P_s = pile shaft perimeter; and δ = pile-soil interface friction angle.

First term in Eq. 2 represents the bottom helix bearing capacity; second term represents the frictional resistance along the interface between the inter-helix soil cylinder and surrounding soil; and third term represents the pile shaft frictional resistance.

The compressive capacity based on IB is given by:

$$Q_c = \gamma`H_2\ A_2\ N_q + \gamma`H_1\ A_1\ Nq + P_s/2\ H_{eff}^2\ \gamma`K_s \tan\delta \qquad (3)$$

where: A_1 = net surface area of the top helix = $\pi(D_h^2\text{-}d^2)/4$

The first term in Eq. 3 accounts for the bearing capacity of the bottom helix; the second term accounts for the bearing capacity of the top helix; and the third term represents the frictional resistance along the pile shaft and the surrounding soil.

Considerations of Pile Settlement and Helix Interaction. To limit the pile settlement to 5%D, especially for piles in dense sand, a reduction factor, R, is applied to the plate bearing capacity. The reduction factor is a function of the soil strength and helix diameter and is given by:

$$R = 2.255 - 0.0426\ \phi \text{ (for } 45° \geq \phi \geq 30° \text{ with } 15° \geq \psi \geq 0° \text{ and } D_h \geq 500 \text{ mm)}$$
$$R = 1.0 \text{ (for } \phi < 30° \text{ and } \psi = 0°) \qquad (4)$$

The interaction between the helices is considered using a helix efficiency factor, E_H = bearing capacity of a multi-helix pile / sum of bearing capacities of individual helices, for different cohesionless soil strengths and helical spacing values. The helix efficiency factor applies to CS failure as the frictional shear resistance of the soil cylinder has to be transformed into bearing resistance onto the helix that confines the cylinder from the top, i.e., in essence CS failure is an end-bearing failure with E_H that accounts for interaction between the helices. Considering both R and E_H, the compressive capacity of helical piles installed in sand is given by:

$$Q_c = \gamma`H_2\ A_2\ N_q\ R + E_H\ \gamma`H_1\ A_1\ N_q\ R + P_s/2\ H_{eff}^{\ 2}\ \gamma`K_s \tan\delta \qquad (5)$$

2.2 Axial Capacity of Helical Piles in Clay

The compressive capacity based on CS failure is given by:

$$Q_c = P_s\ H_{eff}\ \alpha\ C_{uf} + \pi\ D_{h1}\ (H_2 - H_1)\ C_{uc}\ S_f + C_{ub}\ N_c\ A_2 \qquad (6)$$

where: C_{uf} , C_{uc} , C_{ub} = undrained shear strength along shaft, along soil cylinder, and below bottom helix, respectively; α = adhesion factor along shaft; S_f = inter-helix spacing factor for $S_r > 3$, a function of inter-helix spacing (Zhang, 1999); A_2 = surface area of bottom helix; N_c = bearing capacity factor for cohesive soils; D_h = helix diameter; H_{eff} = effective shaft length= shaft length above top helix – helix diameter; H_1 = depth to top helix; H_2 = depth to bottom helix; P_s = perimeter of pile shaft. The first term in Eq. 6 provides the pile shaft adhesion resistance, the second term

accounts for the resistance along the inter-helix soil cylinder and the third term represents the bearing capacity of the bottom helix.
The compressive capacity based on individual helix bearing is given by:

$$Q_c = P_s H_{eff} \alpha C_{uf} + C_{u1} N_{c1} A_1 + C_{u2} N_{c2} A_2 \quad (7)$$

where: C_{u1} and C_{u2} = shear strength below top and bottom helices, respectively; A_1 = net surface area of the top helix = $\pi(D_h^2-d^2)/4$; *and* H_1 and H_2 = depth to top and bottom helices, respectively. In Equation 7, the first term accounts for the adhesion resistance along the pile shaft, and the second and third terms account for the ultimate bearing capacity derived by the top and bottom helices, respectively. Elsherbiny and El Naggar (2013) suggested that the cylindrical shear failure mechanism is appropriate for piles with helices embedded into cohesive soils for helix spacing up to 3 D, and the load transfer mechanism at failure comprises shear along the pile shaft, shear along the inter-helix soil cylinder, and end bearing on the bottom helix.

Axial Capacity of Helical Piles in Structured Clay. The capacity of helical piles in structured and sensitive clays is affected by its installation, which can cause disturbance to soil within the zone affected by the pile helices. This disturbance is attributed to the advancement of the pile shaft into the ground and the rotation of the helical plates, which weakens the soil at the pile interface (Mooney el al. 1985; Bradka, 1997; Zhang, 1999), and the disturbance caused by shaft advancement is even more severe. The soil disturbance can be ascribed to different phenomena: the helical plates disturb soil through spirally shaped cut with intervals equal to the pitch distance and the soil traversed by the helix is sheared, and the shaft displaces the soil laterally. Bagheri and El Naggar (2016) investigated different failure patterns for helical piles installed in structured clays utilizing the results of full-scale uplift and compression load tests data. They concluded that the helical piles' capacity is significantly affected by soil disturbance induced by penetration of pile shaft and proposed a methodology for evaluating the axial capacity of helical piles installed in cohesive soil accounting for soil disturbance.

3 Response of Helical Piles to Lateral Loads

The response of a laterally loaded helical pile can be predicted using three different approaches: (i) beam on Winkler foundation (BWF) method, which treats the soil as a series of disconnected springs, (ii) continuum approach, which considers the soil as a semi-infinite space, and (iii) numerical methods (e.g., finite element) that discretize the soil domain into elements. The BWF method simplifies the analysis of piles nonlinear behaviour with reasonable accuracy for practical applications using discrete nonlinear soil springs (Juirnarongrit and Ashford, 2006; Brandenberg et al. 2007). The background of BWF method is discussed herein**.**

3.1 Beam on Winkler Foundation (BWF)

The soil is simulated as a series of unconnected linear-elastic on nonlinear distributed springs. It assumes that the soil deflection at a given point is proportionally related to the contact pressure at that point and is independent of the contact stresses at other points. The coefficient of subgrade reaction, k, is the ratio between the soil pressure, p, at any given point of the contact surface and the displacement, y, produced by the applied load at that point, i.e. $k = p/y$. The soil modulus of subgrade reaction, $E_s = p/y$ has units of (F/L2) and p is the soil reaction per unit pile length (F/L). E_s depends on the soil type, depth, and pile diameter, d, and is evaluated from field tests on piles. Vesić (1961) performed analyses of beams resting on an elastic, isotropic half-space medium and proposed a relationship between Es, and the material properties in the elastic continuum as:

$$\mathbf{E_s} = \frac{0.65E}{(1-\mu_s^2)}\left[\frac{Ed^4}{E_P I_P}\right]^{1/12} \qquad (13)$$

where E = soil modulus of elasticity, μ_s = soil Poisson's ratio, and E_P I_p is pile flexural rigidity. This model is suitable for medium to long piles.

p-y Curve Method

To account for soli nonlinearity, Matlock (1970) introduced the p-y curve method in which a series of nonlinear soil springs as shown in Figure 2, known as p-y curve, are used to simulate the soil behaviour. The p-y curve is a force-deflection relationship that relates the soil resistance, p, to the pile deflection, y.

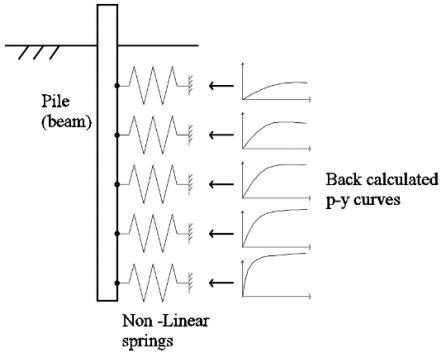

Figure 2. Schematic of the p-y curve method

The p-y curves are established based on the results of lateral load tests conducted on full scale instrumented pile. The bending moment distribution along the pile shaft is calculated based on the pile curvature derived from the strain gage data. The soil reactions and pile deflections are determined by double integration and differentiation of the bending moment. Thus, variation of soil resistance with pile deflection, i.e. p-y

curve, can be assessed at any given depth. Various p-y curves were obtained by curve fitting the results of testing piles embedded in clay and sand (McClelland and Focht 1958; Matlock 1970; Reese et al. 1975; Murchison and O'Neill 1984). The results of field tests verified the suitability of empirical p-y curves for predicting the piles lateral response, but the accuracy is sensitive to the implemented p-y curves. Proper selection of adequate p-y curves is crucial for improving accuracy using this method (Reese and Van Impe, 2001). The behavior of laterally loaded pile is influenced by soil properties, pile type, cross-section shape and flexural stiffness, pile head fixity condition and type of loading. These important parameters are intrinsic characteristics of the developed p-y curves (Juirnarongrit and Ashford, 2006).

p-y Curves of Helical Piles in Structured Clay: Elkasabgy and El Naggar (2019) conducted lateral load tests on full-scale helical piles installed in structured cohesive soil. They load tested five helical piles 6.0 and 9.0 m long with shaft diameter, d =324 mm. The piles were either single or double-helix, with D_h = 610 mm and inter-helix spacing of 1.5 and 3.0 D_h. The piles were instrumented with strain gauges welded on the pile inner wall. The geometrical and material characteristics of the test piles are provided in Table 1. The testing program comprised two phases. In Phase I, the 6.0 m helical piles (SS11, SD11 and SD21) were tested 2 weeks after installation. In Phase II, the 9.0 m helical piles (LS12 and LD12) were tested 9 months after installation. The Phase I testing evaluated the pile behavior in disturbed soil disturbance due to pile installation, and Phase II testing evaluated the pile behaviour after soil regained most of its original strength. The load was applied using a 800 kN hydraulic jack.

The piles' load-displacement curves are displayed in Figure 3. The piles response was generally nonlinear with an initial elastic region extending to a displacement of 1.5 to 2% d, and the final region (almost failure) initiated at displacement of 0.1d. The piles separated from the soil during the loading forming a gap behind the pile, which indicated that the soil has experienced plastic deformations.

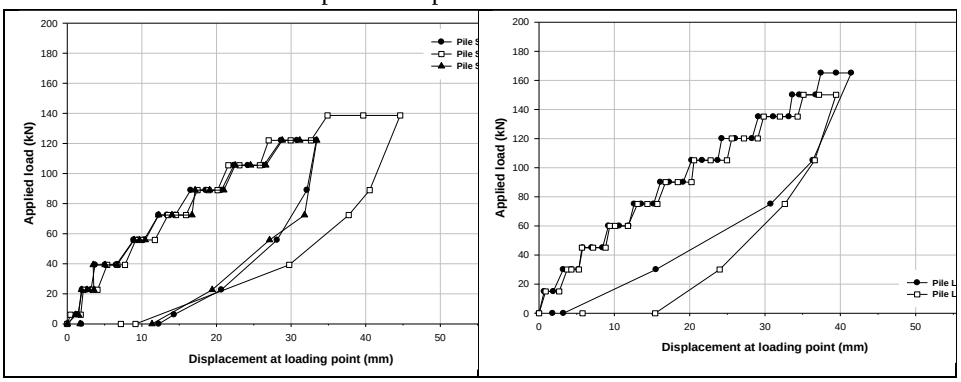

Figure 3. Test results for: a) for 6.0 m piles (Phase I); b) 9.0 m piles (Phase II)

The bending moment profile was evaluated from measured strains. The bending moment profile exhibited a maximum value at a depth of about 5d below the ground elevation, and decreased to zero at the helices. Figure 4 displays the soil resistance along the pile shaft, corresponding to lateral displacement of pile head of 4.0, 6.25 and 12.5 mm. observed maximum soil resistance occurred at a depth of about 3d, then decreased rapidly with depth. The soil resistance for pile LD12 (Phase II) was higher than that for pile SD11 (Phase I). The soil p-y curves and its initial modulus of subgrade reaction were back-calculated from the strain measurements. It was found that soil disturbance during pile installation had a significant effect on the soil resistance and subgrade modulus, regardless of the number of helices and the value of the inter-helix spacing to helix diameter ratio. The effect of soil disturbance was introduced as a disturbance factor that can be incorporated in design. The p-y curves were numerically examined and a favorable agreement was achieved between the predicted and measured distributions of bending moments and deflections.

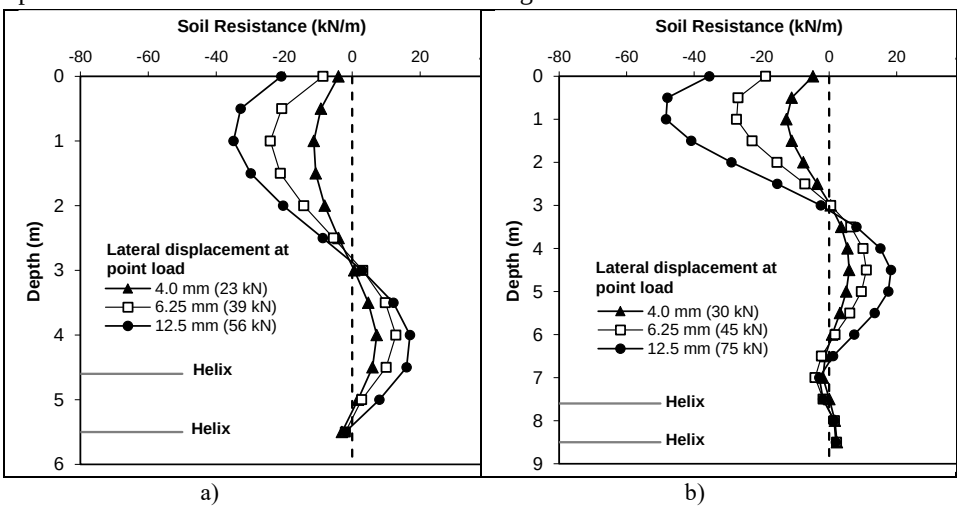

Figure 4. Distribution of soil resistance for piles: a) SD11 and b) LD12

4 Dynamic Behavior of Helical Piles in Clay

Elkasabgy and El Naggar (2013, 2018) conducted full-scale dynamic load tests on helical and driven steel piles to evaluate their dynamic performance characteristics. The test piles were close-ended steel shafts with outer diameter of 324 mm. The piles were subjected to harmonic loading of increasing intensities and varying frequency. The dynamic properties of the subsurface soil were determined using the seismic cone penetration technique. A steel test body (59 machined circular steel plates) was added on top of the pile cap. The excitation force was produced by means of a mechanical oscillator mounted over the test body. The excitation force was harmonic with

frequency between 3 and 60 Hz and was varied by altering the degree of eccentricity of rotating unbalanced masses with a maximum force of 23.5 kN. In addition, lateral free vibration tests were conducted on two piles. The vibration was monitored using two uniaxial piezoelectric accelerometers and one triaxial accelerometer, and the frequency was measured using a tachometer. The accelerometers were located on the test body such that two uniaxial accelerometers were mounted at equidistant positions from the foundation centre on the axis of symmetry. The triaxial accelerometer was mounted on the test body side, at the elevation of its CG. The displacement responses derived from the accelerometers measurements. The pile inner wall was instrumented with strain gauges to measure strain along the pile. Each level of gauges encompassed four half bridges allocated equidistantly from each other.

4.1 Vertical Vibration Tests

Phase I testing involved dynamic experiments conducted on 6.0 m helical and driven piles two weeks after installation. Phase II testing was conducted nine months after installation to allow the disturbed soil to regain some of its original stiffness and strength. Initially, low amplitude load was applied to avoid strong nonlinearity and the load frequency ranged from 3 to 60 Hz. The tests were conducted at five different load amplitudes (0.091, 0.12, 0.16, 0.18, and 0.21 kg.m) for the helical pile and three amplitudes (0.091, 0.16, and 0.21 kg.m) for the driven pile. The steady state dynamic response was measured over the frequency range for the assigned load amplitudes.

Figure 5 displays the test piles vertical response curves. The response varied with frequency and exhibited a resonant peak of 0.4 mm and 0.31 mm for the helical pile in Phases I and II and 0.32 mm for the driven pile in Phase I. As time passed (9 months after installation), the disturbed soil regained stiffness and the helical pile stiffness increased and its resonant frequencies increased by 16 to 26 % and resonant amplitudes decreased by 22 to 55 %. The driven pile response was close to that of helical pile in Phase I, which indicates that the dynamic response is dominated by the shaft resistance. The response curves demonstrated slight nonlinearity, especially for helical pile in Phase II where the measured resonant frequency shifted from 38 Hz for the lower excitation intensity to 35 Hz for the higher intensity.

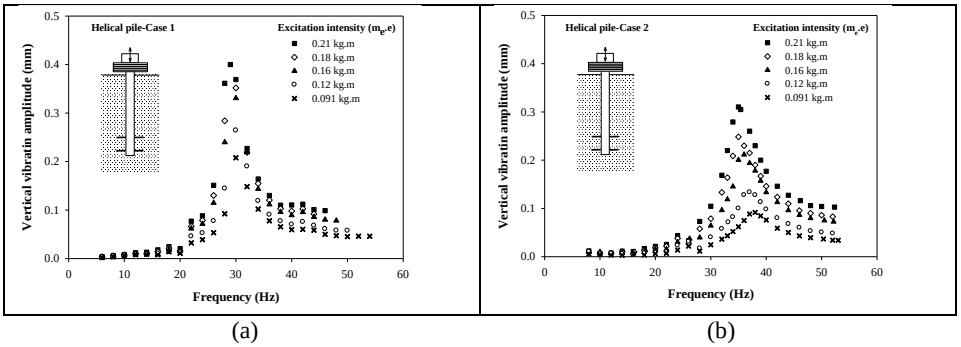

(a) (b)

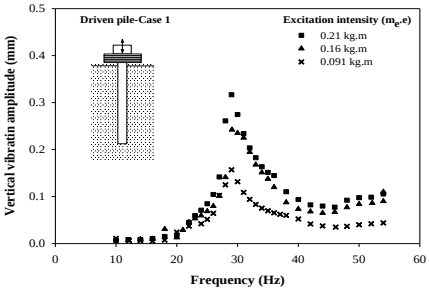

(c)

Figure 5**.** Vertical response curves: a) helical pile (Phase I); b) helical pile (Phase II); and c) driven pile (Phase I)

4.2 Horizontal Vibration Tests

Free vibration Test

The acceleration traces measured during the free vibration tests of piles LD1 (Phase II) and D1 (Phase I) are shown in Figure 6. The piles natural frequencies were obtained from the period of the acceleration cycles and were found to be about 6.7 Hz and 3.0 Hz for piles LD1 and D1, respectively. The piles damping was determined from the decay in the acceleration amplitudes using the logarithmic decrement method. The equivalent viscous damping ratio, Ds, was varied between 4.5% and 6.0% for pile LD1 and 4.6% and 8.0% for pile D1.

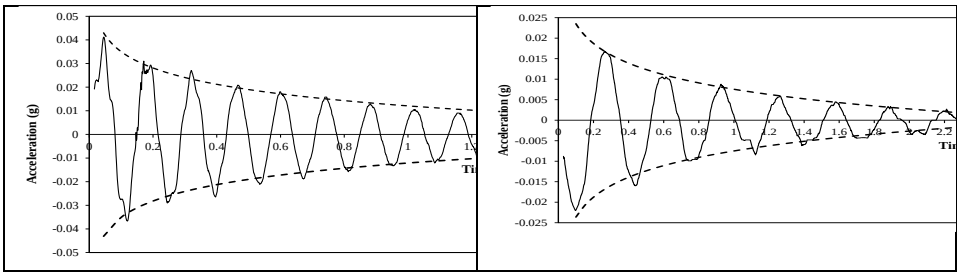

Figure 6. Results of free vibration tests using test body 1;a) helical pile LD1-Phase II and b) driven pile D1-Phase I

Forced horizontal vibration

Figure 7 and Figure 8 present the measured horizontal harmonic response curves for tested helical and driven piles. The response curves displayed two resonant peaks: The first dominated by the horizontal vibration mode and the second associated with the rocking vibration mode. The resonant frequencies decreased as the load amplitude increased due to moderate nonlinearity. The resonant frequencies of helical piles LS1 and LD1 tested in Phase II using test body 1 varied from 3.90 Hz to 3.80 Hz and 4.15 Hz to 3.75 Hz, respectively; and varied from 6.67 Hz to 6.42 Hz and from 6.95 Hz to

6.55 Hz, respectively, when tested with test body 2. The gap formed at the pile-soil interface at ground surface caused the observed nonlinear response. Their maximum horizontal amplitudes with test body 1 were 1.1 mm and 1.13 mm, and 1.78 mm and 1.87 with test body 2. The response of piles LS1 and LD1 was basically the same, indicating that the number of helices had no appreciable effect on the horizontal response. It should be noted that the depth of the upper helix of piles LS1 and LD1 was about 8.5 m (14D) and 6.7 m (11D) below the ground surface. The maximum amplitudes measured for piles LD1 and D1 (Phase I) using test body 1 were 0.85 mm and 1.17 mm, respectively. Figure 7 shows that the resonant frequencies for helical pile LD1 were approximately 3.5 Hz to 4.0 Hz, and were close to the resonant frequencies recorded for the driven pile D1. In addition, the maximum resonant amplitude for pile LD1 was close to the resonant amplitude for pile D1.

The measured resonant amplitudes and frequencies of pile D1 tested in Phase I are compared with those of helical piles LS1 and LD1 tested in Phase II to quantify the regain in soil stiffness. The resonant frequencies increased by 8 to 15 % and resonant amplitudes decreased by 7 to 29 % due to increase in stiffness. The soil stiffness was attributed to thixotropic hardening with time after installation.

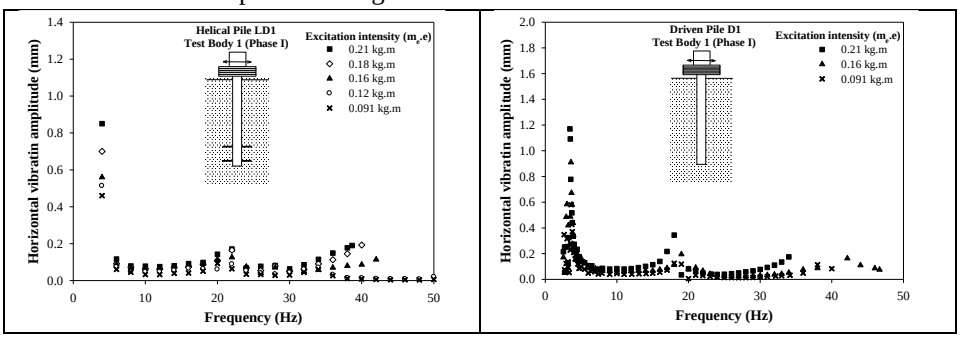

(a) (b)

Figure 7. Measured horizontal response curves for piles tested in Phase I using test body 1; a) helical pile-LD1 and b) driven pile-D1

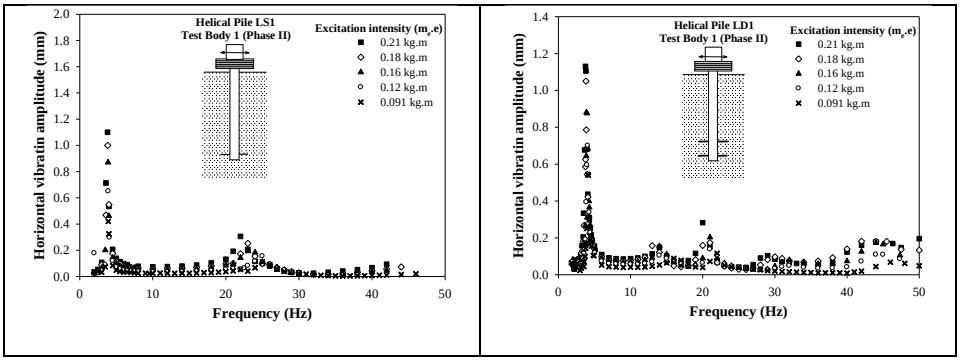

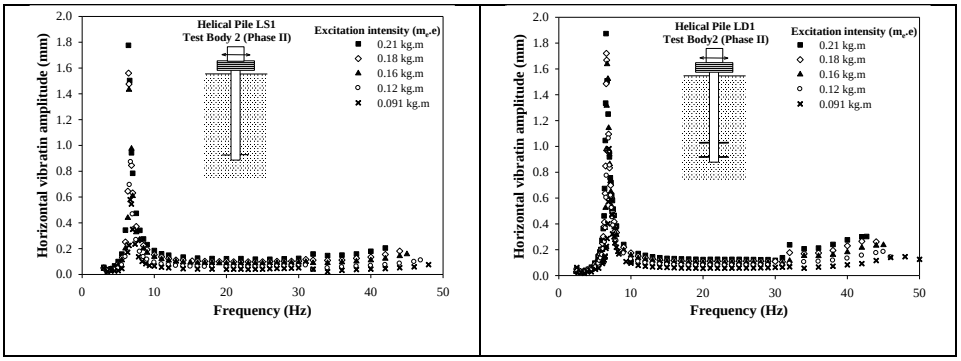

Figure 8. Measured helical piles horizontal response curves in Phase II using test body 1;a) LS1 and b) LD1 and test body 2 c) LS1 and d) LD1

5 Dynamic Response of Helical Piles in Sand

Elshirbiny et al. (2017) conducted lateral dynamic load tests on a full-scale helical pile. The pile was 4.0 m long, shaft diameter d = 114.3mm, wall thickness, t = 8.6mm, and had a single helix with diameter, D = 254mm. The pile head displacement rotation and cceleration were measured using linear string potentiometers, and unidirectional accelerometers. The pile was installed in soil pit 20x20m and 9m deep. The pit was filled with an uncontrolled granular soil fill. Two seismic cone penetration tests (SCPTs) were conducted to measure shear wave velocity. The shear wave velocity (V_s) measured was 900m/s for the top 1.5 m and 300 m/s below that depth. The dynamic load was applied using a 320kg eccentric mass shaker. The shaker was controlled by a variable frequency drive (VFD). It was attached to a 38mm thick steel plate pinned to the test pile (SH2) while supported vertically on a roller supports, which were attached to reaction piles at the back such that the lateral load was transferred to SH2. The shaker was operated up to a speed of 316 rpm (i.e. 5Hz) with force amplitude, f = 4.7kn for SH2. The cyclic test setup involved two single acting hollow hydraulic jacks with capacity 60ton each situated against opposite sides of a steel plate. In order to apply two-way cyclic loading, one jack was pressurized and the other jack had zero pressure, and then reversed. The load was measured using two 900 kN hollow load cells with full-bridge strain gages.

Figure 9a presents average steady-state displacement response at different exciting frequency. The average displacement gradually increased as the load amplitude increased. The mean displacement was not zero especially at speeds ≥ 2.5Hz. As the number of cycles increased at the same frequency, the pile response increased, and its stiffness decreased due to gap forming around the pile rather than changes in the soil stiffness. This was confirmed as the pile returned to its original position when the dynamic load was terminated. Five two-way load cycles were applied with gradually increasing amplitudes. The test was terminated when the maximum hydraulic jack stroke was reached. The cyclic load-displacement curve is shown in Figure 9b. The cyclic loading reduced the pile stiffness.

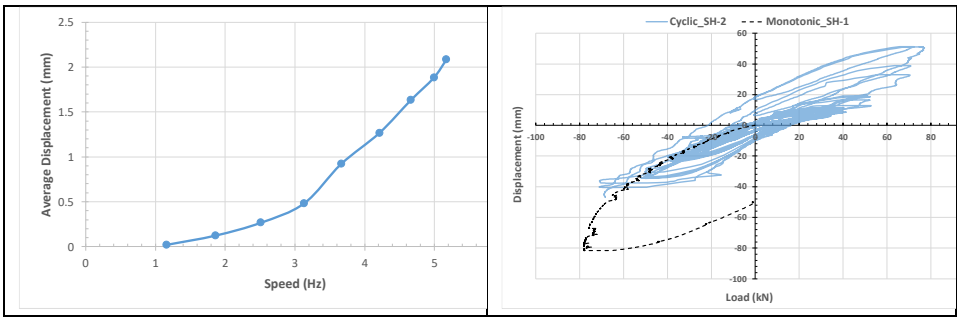

Figure 11. a) Average steady-state response; b) Cyclic load-displacement curve for SH-2

6 Seismic Loading of Helical Piles

6.1 Single Piles in Dry Sand

Elsawy et al. (2019a&b) investigated the seismic response of helical piles embedded in dry sand. They conducted seismic shaking on ten full-scale helical and driven piles using the Large High Performance Outdoor Shake Table (LHPOST) at the University of California – San Diego. The effects of seismic load intensity and frequency on piles response were investigated. Nine steel helical piles and one steel driven pile were installed in well-graded, dense sand compacted to Dr = 100% inside a laminar shear box (6.7 m long, 3.0 m wide and 4.7 m high). The piles were instrumented with six or seven pairs of strain gauges placed at pre-determined elevations. The soil shaking was captured using 23 accelerometers placed within the soil bed. Pile heads were instrumented with accelerometers. Table 1 presents the piles properties.

Table 1. Tested Pile Information

Pile ID	Type (*Notation*)	Length (m)	Helix level (m)	Helix diameter (m)	Diameter/Wall thickness (mm)	Inertia (m^4) x 10^{-6}	Yield Strength (MPa)	Mass (kg)
P1	helical (*88C1HP*)	3.96	3.40	0.254	88 / 5	1.199	450	770
P2, P3	helical (*88C1HP*)	3.66	- 3.15	0.254	88 / 5	1.199	450	750 780
P4	helical (*88C2HP*)	3.66	- 2.55	0.203 0.254	88 / 5	1.199	450	750
P5	Driven (*88CDP*)	3.66	---	---	88 / 5	1.199	450	370
P6	helical (*76S1HP*)	3.66	- 3.15	0.254	76 / 5	1.257	415	435

*C: circular shaft, S square shaft, 1HP & 2HP: single helix & double helix pile

The seismic loading tests consisted of two different shaking schemes: white noise records and ground motion records. The white noise contained a range of frequencies (0 – 40 Hz) and had a peak acceleration of 0.15 g. The ground motion records used were: Northridge (1994) and Takatori (1995) earthquakes. To observe both the linear and non-linear behavior of piles, each earthquake record was scaled to 75% and 50% resulting in a total of 6 earthquake records. Northridge record had a frequency range of 1.5 Hz to 5.0 Hz, while Takatori record had a range of 0.5 Hz to 1.5 Hz.

Figure 10 shows the Fourier spectra of pile P1 response obtained for strain gauge and accelerometer readings. Each Fourier spectrum displays two peaks corresponding to two different modes of motion, horizontal and rotational degrees of freedom.

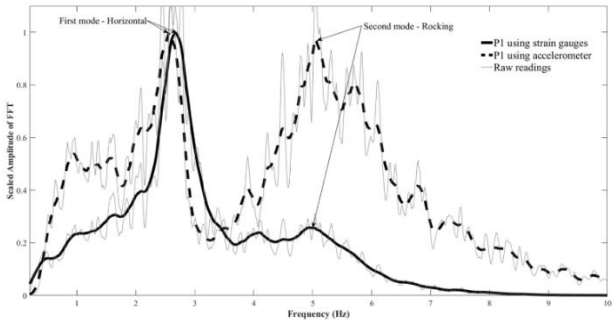

Figure 10. Fourier spectra of Pile 1 response from strain gauges and accelerometer

Figure 11 compares the response of Piles 2, 5 and 6 to two ground motions with equal peak ground acceleration but different frequency content; 100% Northridge and 75% Takatori. All circular helical piles (Piles 1-4), had natural period ranging between 0.47s - 0.53s, which was close to the predominant period of Takatori earthquake; therefore, all circular helical piles had a greater response during Takatori. On the other hand, the driven and the square helical piles had a period of 0.24s and 0.29s, respectively. This coincided with the peak of Northridge; therefore, they had higher response during Northridge earthquake.

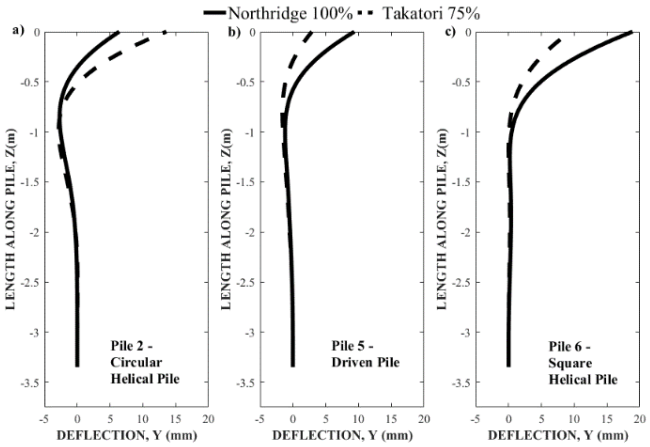

Figure 11. Response to 100% Northridge & 75% Takatori a) Pile 2 b) Pile 5 c) Pile 6

The results showed no clear advantage for the shape of pile cross-section (i.e. square or circular). On the other hand, the response of the double-helix pile was less than that of the single-helix pile due to the negative moment developed close to the location of the second helix. It was also observed that the natural frequency of the driven pile was slightly higher than that of the helical piles. However, the response of the helical pile was very close to that of the driven pile, which illustrates the ability of helical piles to perform as good as conventional piles under seismic loading.

6.2 Helical Pile groups in Dry Sand

Fayez et al. (2021 and 2022) conducted shake table tests on single and grouped helical piles and measured their responses to strong ground motions. They evaluated the effects of earthquake characteristics (i.e., intensity and frequency content) on seismic performance of the single and grouped HPs from the measured responses. In addition, they discussed the performance characteristics of helical pile groups in terms of the interaction between piles within a group and the contributions of vertical and lateral stiffness of individual piles to the rocking stiffness and the overall capacity of the pile group. Single piles as well as two groups of HPs with diameters 88 mm and 140 mm, were subjected to strong ground motions. Each group consisted of four-piles with similar diameters connected to a steel skid filled by sand to simulate a superstructure inertial load. The 88 mm-diameter piles were loaded with 62 kN and the 140 mm-diameter piles were loaded with 98 kN. Accelerometers were placed on the skid at mid-height to record its acceleration. Figure 12 presents the shake table arrangement and Figure 13 depicts the distribution of piles within PG1 and PG2. Table 2 presents the piles dimensions and material properties.

Figure 12. Shake table tests of pile groups

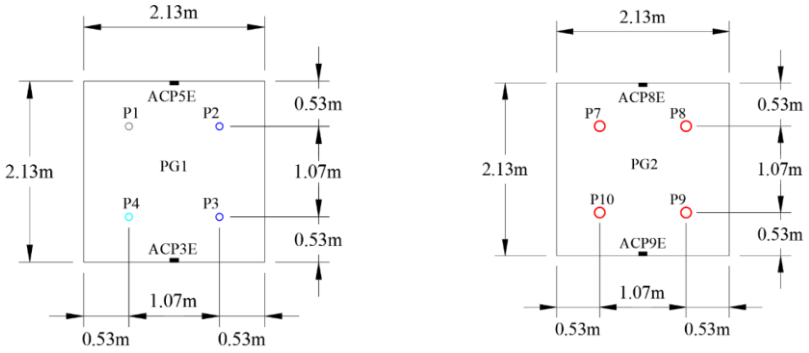

Figure 13 Pile groups: (a) PG1 (b) PG2 .

Table 2 Properties of test piles.

Pile Group	Pile	Type*	Total Length/ Depth (m)	Helix Level / Helix Diameter (m)	Diameter / Wall Thickness (mm)	Yield Strength (MPa)
PG1	P1	H	3.96 / 3.66	-3.51 / 0.254	88 / 5.3	448.2
	P2 P3	H	3.66 / 3.35	-3.20 / 0.254		
	P4	2H	3.66 / 3.35	-2.59 / 0.254 -3.20 / 0.203		
PG2	P7 P8 P9 P10	H	4.22 / 3.35	-3.20 / 0.254	140 / 10.5	551.6

* H (single helical pile), 2H (double helical pile)

Figure 14 compares the bending moment profiles for single piles and piles in a group during Northridge Earthquake with 100% PGA (NOR-100) and Takatori Earthquake with 75% PGA (TAK-75). Single piles experienced resonance during TAK earthquake and exhibited significant response. Even though NOR-100 TAK-75 had the same PGA, the maximum bending moment was more than twice during TAK-75. Moreover, PG1 experienced low bending moment in both earthquakes as it didn't experience resonance. However, it exhibited a slightly larger bending moment during NOR-100 due to the closeness of its natural frequency to the frequency content NOR-100 compared to TAK-75. PG2 exhibited larger bending moment due to resonance during NOR-100. This emphasizes the importance of considering the earthquake frequency content in seismic design of helical pile foundations.

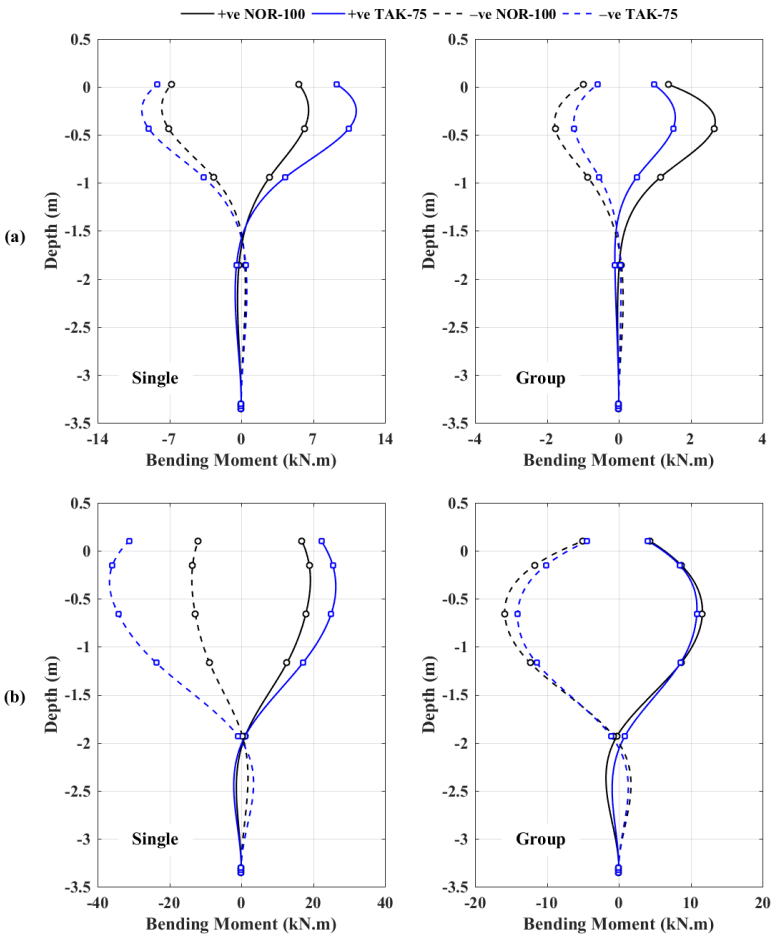

Figure 14. Effect of earthquake frequency content on maximum bending moment profiles for single piles and fixed-head pile groups: P2 (a) and P7 (b).

Rocking Behaviour of Helical Pile Groups

The rocking resistance of the helical piles within a group is an important mechanism to resist the seismic loading. This rocking resistance is a function of the normal force developed in the piles during the seismic event. Figure 15 presents the variation of maximum normal forces with PGA. Fig. 15a shows higher increase in normal force for larger diameter pile group (PG2) as the higher flexural rigidity of the piles promoted the rocking behaviour over lateral deflection. In addition, larger normal forces were observed during resonance (NOR earthquake) for both pile groups. On the other hand, Figure 15b shows that the rate of increase in maximum normal force was lower than the increase in PGA for both pile groups. However, the rate of increase when resonance was experienced was higher. This indicates that rocking behaviour increased during resonance and consequently, the normal forces increased.

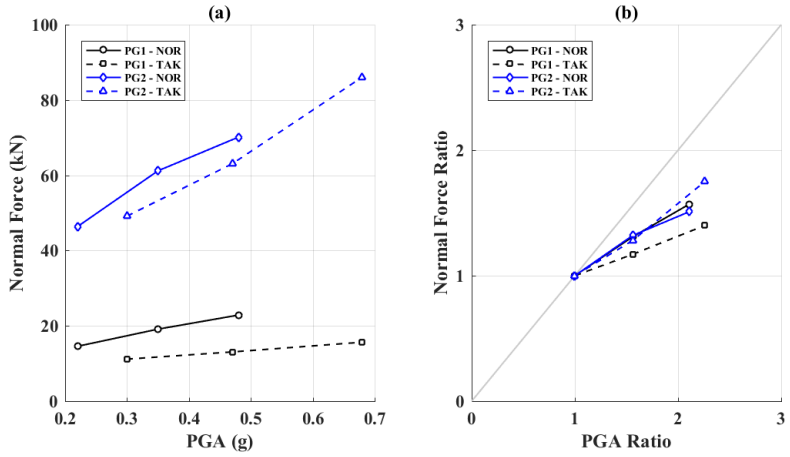

Figure 15. Variation of maximum normal force with PGA for fixed-head pile groups: actual values (a) and normalized correlation (b).

6.3 Seismic Response of Helical Piles in Liquefiable Soil

Hussein and El Naggar (2021) investigated the seismic performance of helical piles in liquefiable soil employing three-dimensional nonlinear finite element models. The numerical models were validated using the published results from a comparative shaking table testing program of identical 4-pile groups installed in saturated and dry sand. The validated models were then used to analyze the seismic lateral and axial responses of helical piles to investigate the soil-helical pile-superstructure interaction.

The helical pile groups considered in the numerical models were installed in a soil profile comprising a surficial clay layer, loose sand layer and dense sand layer as shown in 错误!未找到引用源。6. The soil profile was dry in one set and saturated with water in the other set of shakings so that pore water pressure could develop during the shaking, and liquefaction could occur. The identical soil-pile group configura-

tion in both sets of experiments allowed a direct comparison between the non-liquefiable and liquefiable tests. The soil bed was enclosed in a laminar box with dimensions of 3.2m x 2.4m x 3.1m, which was situated on a 6mx6m shaking table. The soil bed considered in the numerical modeling consisted of three layers: 0.3m clay crust, 1.2m loose sand with D_r = 60%, and 1.6m dense sand with D_r = 90%. Table 3 describes the configuration of the analyzed helical pile group (HPG). The 1.95m long HP shaft was divided into elements aligned with the adjacent soil elements. **错误!未找到引用源。** summarizes the layout of the soil elements, HP, cap, and superstructure, as well as elements types and material models.

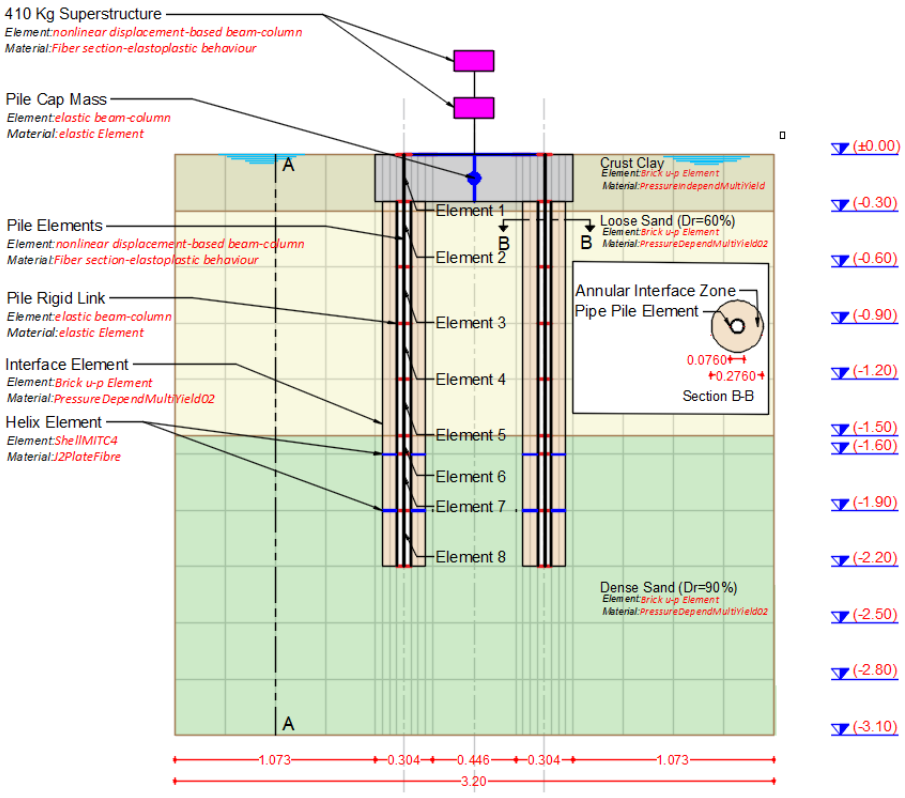

Figure 16 Longitudinal section of soil-pile-superstructure interaction numerical model

Table 1. Helical pile group configuration, units in mm

Parameter	(mm)	Parameter	(mm)	Parameter	(mm)
Pile d	76	Helix Spacing	300	Pile Cap Thick	250
Shaft Wall Thickness	5	Pile Spacing	750	Helix Thick	10
Helix D_{helix}	228	Pile Cap width	1050		

The soil-helical piles-superstructure interaction models were developed using the OpenSees platform (Mazzoni et al. 2006). The test soil bed was discretized into 5148 elements. The soil elements were appropriately refined adjacent to the piles. The maximum elements' sizes in the longitudinal direction (A_s =3.6m) and transversal (B_s = 2.4m) direction were 0.27m and 0.34m, and the largest element size along the depth (d_s=3.1m) was 0.3m. The element size allowed a shear wave with maximum frequency to propagate efficiently considering shear wave velocity, V_s = 100m/sec, at maximum frequency $F_{max}=V_s/(4H)$ = 73.5Hz (H = 0.34m). The shaft was divided into elements aligned with the adjacent soil elements and rigid link elements were applied perpendicular to the shaft to fill the pile volume within the soil. The helix (D_{helix}=0.228m) was divided into elements of the same size as the surrounding soil elements, which facilitated the contact between HP and adjacent soil elements. The top and bottom helices were placed at a depth of 1.6m and 1.9m, respectively.

The soil was discretized using 8-node hexahedral linear isoperimetric elements (Brick u-p Element) (Yang et al. 2008). The elastic-plastic pressure dependant constitutive model PressureDependMultiYield02 (PDMY02) simulated the nonlinear sand response. PressureIndependMultiYield elastic-plastic material model simulated the clay crust, in which the plasticity is considered in the deviatoric stress-strain response but does not account for the confining pressure variability (Elgamal et al. 2002). The interface element was 10cm thick to simulate the large relative stiffness between the soil and helical piles. The measured soil parameters in the shake table tests were employed to correlate the material model geotechnical parameters. The particles' mean diameter and uniformity coefficient were used to calculate the maximum and minimum voids ratios (Sarkar et al. 2019), which were correlated to the low strain shear modulus at each depth (Das and Ramana 2011). The geotechnical parameters were adjusted through the calibration process to capture the proper soil element response.

Figure 17 compares the pile calculated lateral displacement of single helical pile (SHP) and double helical pile (DHP) with that for RC pile (RCP) of equivalent lateral stiffness. The lateral displacements of SHP and DHP were less than that for RCP in both saturated and dry tests. The higher axial stiffness of the HPs and the fixation provided by the helices increased the rocking and flexural resistance of the HPG. This is because the top helix offered significant resistance (and fixation), which reduced the rotation of the second helix. Thus, the contribution of the helices to lateral resistance is primarily due to passive resistance associated with their rotation (Elkasabgy and El Naggar 2019). Similarly, Al-Baghdadi et al. (2015) investigated the helix contribution to the lateral resistance and concluded that the contribution is important only for helical plates placed close to the surface. In addition, the flexural deformation was primarily concentrated within the liquefied layer.

The axial force was higher in the DHP shaft than the SHP at the top helix location; therefore, the axial force at the bottom helix decreased even more than the case for SHP. This response refers to the ability of the DHP to resist higher axial loads compared to the SHP. The shaft axial force below the bottom helix was marginal. These observations are further elaborated by monitoring the shaft friction and helix bearing forces. The shaft force within the loose sand decreased rapidly as the shaking progressed and diminished as liquefaction occurred. The static shaft force of the SHP

was greater than that of the DHP, while its bearing force was less than the DHP. The end bearing forces for SHP and DHP increased to compensate for the reduction in the shaft forces. Thus, the bearing forces fluctuated as the shaft friction fluctuated, which was accompanied by pile. Cycles of tensile forces also occurred in both the leading and trailing DHP, which demonstrates that the complicated behaviour of HPs during the generation and dissipation of excess pore water pressure (EPWP). For both SHP and DHP, the shaft friction diminished as the shaking progressed and became zero (and even negative friction) at the end of motion due to the liquefaction of loose sand. On the other hand, the total bearing resistance increased, which compensated for the shaft friction and maintained the overall capacity of the pile. In addition, there was an appreciable difference in bearing forces of the leading and trailing piles due to the rocking of the pile group. Hussein and El Naggar (2022a) further extended this study to consider the behavior of prototype helical piles and reported similar findings.

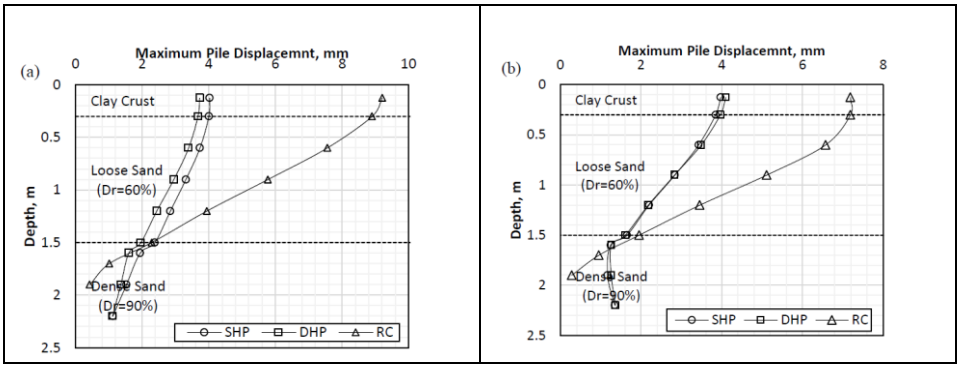

Figure 17 Piles maximum lateral displacement for SHP, DHP and RCP during the 0.18g Wolong motion: (a) saturated test; (b) dry test

Hussein and El Naggar (2021) concluded that the seismic lateral displacements of helical piles and associated soil were lower than those for RC piles. The helical pile groups exhibited rigid body movement in the saturated soil, especially DHPs, as the dense sand liquefied. In addition, the helical pile seismic settlements were much less than that of the RCP for both the saturated and dry soils. As liquefaction occurred, the HP shaft resistance diminished, and the pile settled. However, higher end-bearing force was mobilized, which compensated for the decrease in shaft force, which demonstrates the excellent performance of helical piles in maintaining their capacity during and after liquefaction and controlling the post-liquefaction settlement. Finally, the helical pile response in the saturated test was dominated by the rocking behaviour, while the flexural behaviour dominated the response in the dry tests.

6.4 Seismic Response of Helical Piles in Cohesive Soil

Hussein and El Naggar (2022b) evaluated the dynamic response of driven and helical piles in cohesive soil. They developed three-dimensional (3D) finite element models (FEMs) to analyze the response of driven piles based on the results of a full-scale

field tests conducted by Fleming et al. (2016). These large-scale field tests examined the seismic response of driven piles in unimproved and improved soft clay.

Figure 18a presents a longitudinal section of the field test with the location and dimensions of the improved soil. The soil elements were simulated using 8-node hexahedral linear isoperimetric elements (Brick u-p Element). The element is used to simulate the dynamic response of the soil-fluid coupled material. The unimproved and improved clay materials were simulated using PressureIndependMultiYield elastic-plastic material model. In this model, the plasticity appears in the deviatoric stress-strain response only. For the volumetric response, it is independent of the deviatoric stress in the linear elastic response and is insensitive to the confining pressure variation. On the other hand, the sand layer was simulated using PressureDependMultiYield02, which is an elastic-plastic model that is sensitive to the change in the confining pressure. The FEM was validated by comparing its predictions with the measured pile response and bending moment profile during the field tests.

The validated FEM was employed to simulate the dynamic response of helical piles. **错误!未找到引用源。** 18b presents the longitudinal section of the helical pile considered within the soil profile of the field test. Both single-helix and double-helix piles were considered in the analysis. The cross-section of the helical pile pipe cross-section was AISC-HSS12x0.5, and the helix was 762mm in diameter and 25mm in thickness. The bottom helix was placed at the interface of the soft clay-sand layers (i.e., depth 3.4m below the ground), and the pile toe was embedded 150mm in the sand layer. The helical pile was 5.35m long, which was shorter than the driven pile by 1.75m. The second helix was placed above the bottom helix with an inter-helix spacing of 1.5, 2.0, 2.5, and 3.0 times the helix diameter (D_{helix}).

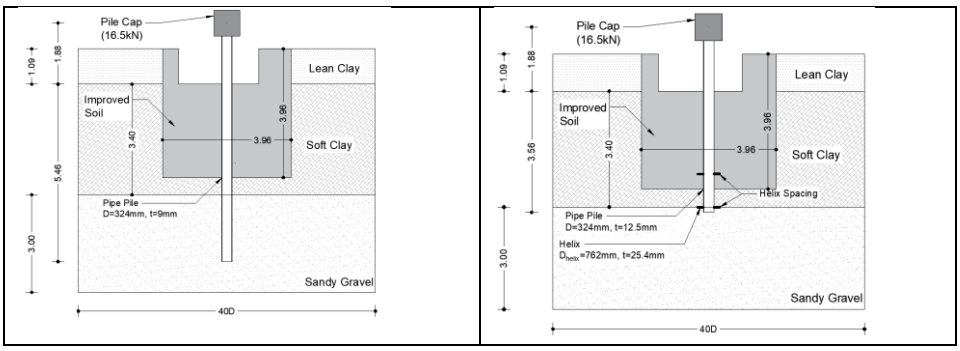

Figure 18 Longitudinal section of the soil-pile profile: a) drive pile; b) helical pile

The driven and helical piles' dynamic lateral responses were calculated and are compared in terms of the force-displacement response at the pile head and at the ground surface as shown in Figure 19. Different analyses were conducted considering a SHP and DHP with helix spacing of 1.5, 2, 2.5 and 3D_{helix}. **错误!未找到引用源。**a shows that the lateral response of the DHP improved as the second helix was placed closer to the ground surface. The displacement of the DHP decreased from 9.6cm to

8.7cm as the inter-helix spacing increased from $1.5D_{helix}$ to $3D_{helix}$. This improvement in lateral response is attributed to the additional bearing resistance offered by the top helix as it was placed within the pile segment that experienced large deflection. This was observed from the axial forces calculated in the pile as will be discussed later. **错误!未找到引用源。**b shows that the lateral displacement of the piles at the ground surface was much lower than at the head because the large free-standing segment of the pile caused most of the displacement, which is not affected much by the helices.

To further evaluate the dynamic lateral performance of driven and helical piles in cohesive soils, the undrained shear strength of the soil (Su) was varied increased to 50KPa, 75KPa, and 100KPa. The maximum shear modulus was also increased with the same ratio of the undrained shear strength. **错误!未找到引用源。** (c, e, and g) present the lateral force-displacement responses of the driven and the helical piles at pile head, while **错误!未找到引用源。** (d, f, and h) display the force-displacement responses at the ground level. As expected, the pile lateral displacements at both the pile and ground surface decrease the soil strength and stiffness increase. The driven pile lateral displacement decreased from 8.7cm at Su=25KPa to 3.9cm at Su=100KPa. Similarly, the SHP lateral displacement decreased as the soil strength increased, i.e., decreased from 10cm at Su=25KPa to 3.9cm at Su=100KPa. The lateral response was enhanced further by using the DHP; for example, the maximum lateral displacement at the DHP head decreased from 8.7cm at Su=25KPa to 3.6cm at Su=100 KPa (i.e., performed better than the driven pile).

Hussein and El Naggar (2022b) concluded that the lateral displacement of DHP was the same as or less than that of the driven pile for the same dynamic loading applied at the pile head. The lateral response of helical piles improved as the clay shear strength increased due to the additional passive resistance on the helices. They also concluded that during a seismic event, the helical pile would experience lower lateral deformation and bending moment compared to the driven pile due to the kinematic interaction. Furthermore, for piles fully embedded in the ground, the seismic performance of helical piles was better than that of the driven pile.

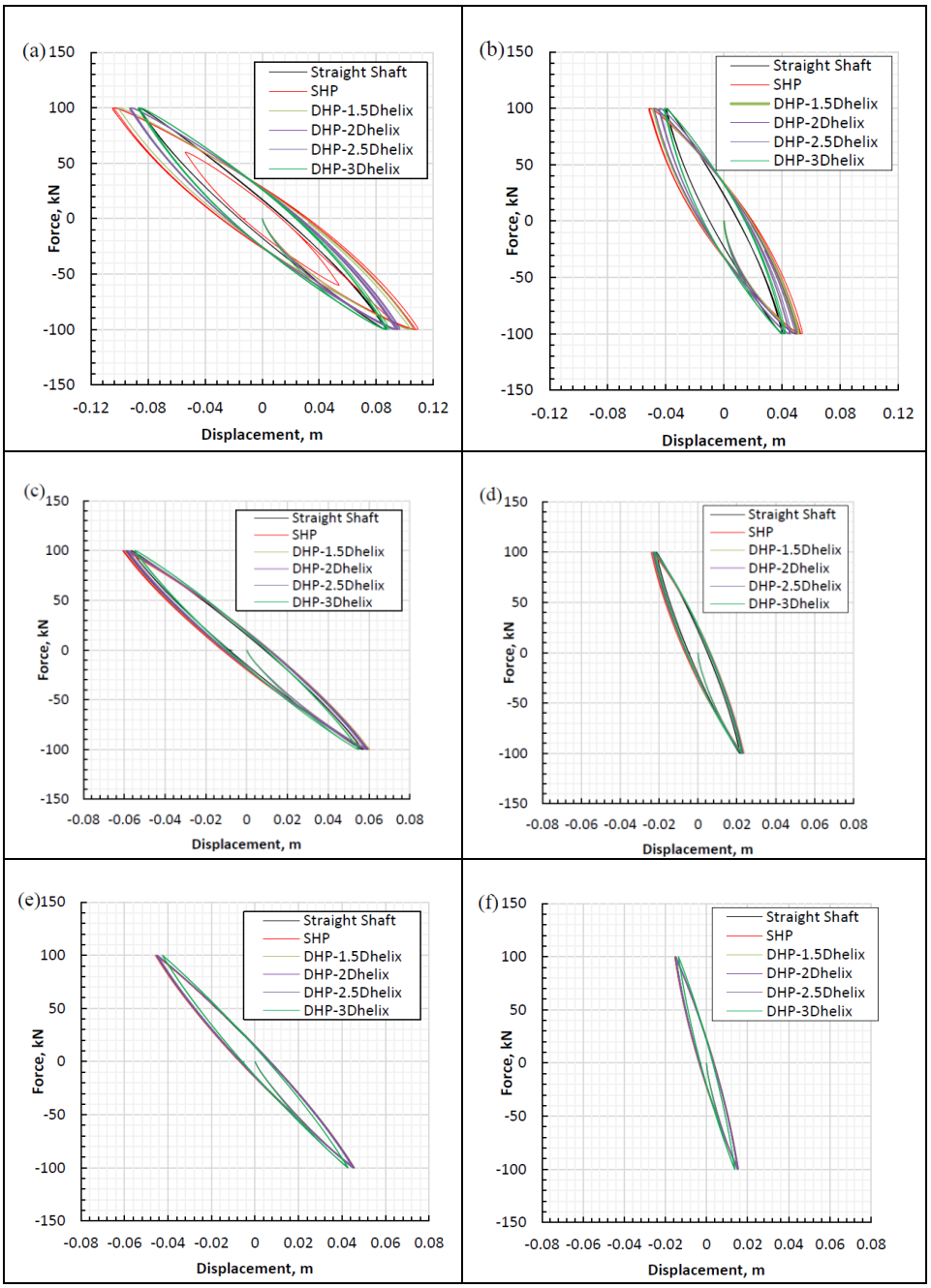
(a)
(b)
(c)
(d)
(e)
(f)
Straight Shaft
SHP
DHP-1.5Dhelix
DHP-2Dhelix
DHP-2.5Dhelix
DHP-3Dhelix
Force, kN
Displacement, m

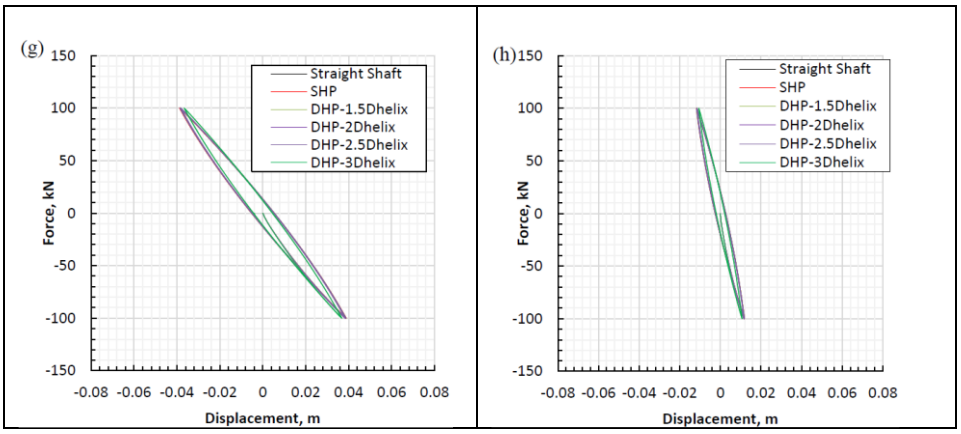

Figure 19 Force-Displacement hysteretic loops in the test with cohesive clay: At pile head (a) Su=25KPa; (b) Su=50KPa; (c) Su=75KPa; (d) Su=100KPa, and at the ground level (e) Su=25KPa; (f) Su=50KPa; (g) Su=75KPa; (h) Su=100KPa

References

1. Alwalan, MF. and El Naggar, MH. 2021. Load-transfer mechanism of helical piles under compressive and impact loading. ASCE International Journal of Geomechanics, Doi.org/10.1061/(ASCE)GM.1943-5622.0002037.
2. Alwalan, M.F. and El Naggar, M.H. 2020. Analytical models of impact force-time response generated from high strain dynamic load test on driven and helical piles. Computers and Geotechnics, Vol 128, DOI:10.1016/j.compgeo.2020.103834.
3. Alwalan, M.F. and El Naggar, M.H. 2020. Finite element analysis of helical piles subjected to axial impact loading. Computers and Geotechnics, Vol. 123, DOI 2020.103597.
4. Ashford, S. A., Juirnarongrit, T., Sugano, T. and Hamada, M. 2006. Soil-pile response to blast-induced lateral spreading. I: field test. Journal of Geotechnical and Geoenvironmental Engineering, 132(2), 152–62.
5. Bagheri, F. and El Naggar, M.H. 2016. Effects of installation disturbance on behavior of multi-helix piles in structured clays. Journal of Deep Foundations, 9(2), pp. 80-91.
6. Bradka, T.D., (1997). Vertical capacity of helical screw anchor piles. Master of Engineering Report, University of Alberta, Alberta, Canada.
7. Brandenberg SJ, Zhao M, Boulanger RW, Wilson DW (2013) p-y plasticity model for nonlinear dynamic analysis of piles in liquefiable soil Journal of geotechnical and geoenvironmental engineering 139:1262-1274.
8. Elgamal A, Yang Z, Parra E (2002) Computational modeling of cyclic mobility and post-liquefaction site response Soil Dynamics and Earthquake Engineering 22:259-271
9. Elkasabgy, M. and El Naggar, M.H. 2013. Dynamic response of vertically loaded helical and driven steel piles. Canadian Geotechnical Journal, Vol. 50, No. 5, pp. 521-535.
10. Elkasabgy, M. and El Naggar, M.H. 2015. Axial compressive response of large-capacity helical and driven steel piles in cohesive soil. Canadian Geotechnical Journal, 52(2), pp. 224-243.
11. Elkasabgy, M.A. and El Naggar, M.H. 2018. Lateral vibration of helical and driven steel piles installed in cohesive soils. ASCE Journal of Geotechnical and Geoenvironmental Engineering, 144 (9): DOI: 10.1061/(ASCE)GT.1943-5606.0001899.

12. Elkasabgy, M. and El Naggar, M.H. (2019). Lateral performance and *p-y* curves for large-capacity helical piles installed in clayey glacial deposit. Geotechnical and Geoenvironmental Engineering, ASCE, https://doi.org/10.1061/(ASCE)GT.1943-5606.0002063.
1. El-Sawy, M.K., El Naggar, M.H., Cerato, A.B., Elgamal, A. 2019. Data reduction and dynamic p-y curves of helical piles from large scale shake table tests. Geotechnical and Geoenvironmental Engineering, ASCE, Vol 145 (10): 04019075.
13. El-Sawy, M.K., El Naggar, M.H., Cerato, A.B., Elgamal, A. 2019. Seismic performance of helical piles in dry sand from large scale shake table tests. Geotechnique, 69(12), 1071-1085, DOI: 10.1680/jgeot.18.P.001.
14. Elsharnouby, M. and El Naggar, M.H. 2018. Field investigation of lateral monotonic and cyclic performance of reinforced helical pulldown micropiles. Canadian Geotechnical Journal, doi.org/10.1139/cgj-2017-0330, Published on-line Jan 23.
15. Elsharnouby, B. and El Naggar, M.H. 2018. Numerical investigation of axial monotonic performance of reinforced helical pulldown micropiles. ASCE International Journal of Geomechanics, 18 (10) DOI: 10.1061/(ASCE)GM.1943-5622.0001161.
16. ElSharnouby, M.M. and El Naggar, M.H. 2012. Axial monotonic and cyclic performance of fibre-reinforced polymer (FRP) – steel fibre–reinforced helical pulldown micropiles (FRP-RHPM). Canadian Geotechnical Journal, Vol. 49, No. 12, pp. 1378-1392.
17. ElSharnouby, M.M. and El Naggar, M.H. 2012. Field investigation of axial monotonic and cyclic performance of reinforced helical pulldown micropiles. Canadian Geotechnical Journal, 49(5), pp. 560-573.
18. Elsherbiny, Z. and El Naggar, M.H. 2013. Axial compressive capacity of helical piles from field tests and numerical study. Canadian Geotechnical Journal, Vol. 50 (12), 1191-1203.
19. Fahmy, A. and El Naggar, M.H. 2017. Axial and lateral performance of helical tapered piles in clay. Journal of Geotechnical Engineering, Institute of Civil Engineers, UK, Vol 170 (6), pp. 503-516, DOI: 10.1680/jgeen.16.00116.
20. Fahmy, A. and El Naggar, M.H. 2016. Cyclic lateral performance of helical tapered piles in silty sand. Journal of Deep Foundations, 10(3), pp. 111-124.
21. Fahmy, A. and El Naggar, M.H. 2016. Cyclic axial performance of helical tapered piles in sand. Journal of Deep Foundation Institute, DOI: 10.1080/19375247.2016.1211353.
22. Fayez, A., El Naggar, M.H., Cerato, A. and Elgamal, A. 2021. Assessment of SSI effects on stiffness of single and grouped helical piles in dry sand from large shake table tests. Bulletin of Earthquake Engineering, doi.org/10.1007/s10518-021-01241-7.
23. Fayez, A., El Naggar, M.H., Cerato, A. and Elgamal, A. 2022. Seismic Response of Helical Pile Groups from Shake Table Experiments. Soil Dynamics and Earthquake Engineering. Vol. 152, DOI: 107008.
24. Fleming, B. J., Sritharan, S., Miller, G. A., and Muraleetharan, K. K. (2016). "Full-scale seismic testing of piles in improved and unimproved soft clay." *Earthquake Spectra*, 32(1), 239-265.
25. Harnish, J. and El Naggar, M.H. 2017. Large- diameter helical pile capacity torque correlations. Canadian Geotechnical Journal, 54(7), pp. 968-986.
26. Hussein, A.F. and El Naggar, M.H. 2021. Seismic axial behaviour of pile groups in non-liquefiable and liquefiable soils. Soil Dynamics and Earthquake Engineering, 149, DOI:106853.
27. Hussein, A.F. and El Naggar, M.H. 2021. Seismic behaviour of piles in non-liquefiable and liquefiable soil. Bulletin of Earthquake Engineering, 10.1007/s10518-021-01244-4.
28. Hussein, A.F. and El Naggar, M.H. 2022a. Effect of model scale on helical piles response established from shake table tests. Soil Dynamics and Earthquake Engineering. Vol 152, DOI: 107013.

29. Hussein, A.F. and El Naggar, M.H. 2022b. Seismic Performance of Driven and Helical Piles in Cohesive Soil. Acta Geotechnica, submitted.
30. Juirnarongrit, T. and Ashford, SA., 2006. Soil-Pile Response to Blast-Induced Lateral Spreading. II: Analysis and Assessment of the *p–y* Method. ASCE Geotechnical and Geoenvironmental Engineering, ASCE. doi:10.1061/(ASCE)1090-0241(2006)132:2(163).
31. Livneh, B. and El Naggar, M.H. 2008. Axial load testing and numerical modeling of square shaft helical piles, Canadian Geotechnical Journal, Vol. 45, No. 8, pp. 1142-1155.
32. Lutenegger, A. J. (2009). Cylindrical Shear or Plate Bearing? - Uplift Behavior if Multi-Helix Screw Anchors in Clay. International Foundation Congress and Equipment Expo, 456-463.
33. Mansour, M.A. and El Naggar, M.H. 2021. Optimization of grouting method and axial performance of pressure grouted helical piles. Canadian Geotechnical Journal, https://doi.org/10.1139/cgj-2021-0093.
34. Matlock, H. (1970). Correlations for design of laterally loaded piles in soft clay. Proc., 2nd Offshore Technology Conf., Houston, Texas, 577-594.
35. Mazzoni S, McKenna F, Scott MH, Fenves GL (2006) OpenSees command language manual Pacific Earthquake Engineering Research (PEER) Center 264.
36. McClelland, B., and Focht, J.A. (1958). Soil modulus of laterally loaded piles. Transactions of ASCE, Vol. 123, 1049-1063.
37. Mooney, J. S., Clemence, S. P., & Adamczak . (1985). Uplift Capacity of helix Anchors in Clay and Silt. ASCE Convention Conference Proceedings, New York, *ASCE*, 48-72.
38. Murchison, J., & O'Neill, M. (1984). Evaluation of p-y relationships in cohesionless soils: Analysis and Design of Pile Foundations. Proc. of Symp. in conjunction with ASCE National Convention: pp. 174-191.
39. Orang, M.J., Boushehri, R., Motamed, R., Prabhakaran, A. Elgamal, A. 2021. Large-Scale Shake Table Experiment on the Performance of Helical Piles in Liquefiable Soils. Proc., 45th DFI Annual Conference on Deep Foundations, Deep Foundations Institute.
40. Perko, H. A. (2009). Helical Piles: A Practical Guide to Design anf Installation. New Jersey: John Wiley & Sons.
41. Reese, L.C., Cox, W.R., and Koop, F.D. (1975). Field testing and analysis of laterally loaded piles in stiff clay. Proc., 7th Offshore Technology Conf., Dallas, Texas, 672-690.
42. Reese, L.C., and Welch, R.C. (1975). Lateral loading of deep foundations in stiff clay. J. Geotech. Eng. Div., ASCE, 101(GT7), 633-649.
43. Reese, L. C., & Van Impe, W. F. (2001). Single Piles and Pile Group under Lateral Loading (2 ed.). Balkema, Rotterdam.
44. Shahbazi, M., Cerato, A., El Naggar, M. H., Elgamal, A. 2020. Evaluation of seismic soil-structure interaction of full-scale grouped helical piles in dense sand. ASCE International Journal of geomechanics, Vol. 20 (12). doi/abs/10.1061/(ASCE)GM.1943-5622.0001876.
45. Shahbazi, M., Cerato, A., Allred, S., El Naggar, M. H., Elgamal, A. 2019. Damping characteristics of full-scale grouped helical piles in dense sands subject to small and large shaking events. Canadian Geotechnical Journal, doi.org/10.1139/cgj-2018-0769.
46. Tappenden, K. M. (2007). Predicting the Axial Capacity of Screw Piles Installaed in Western Canadian Soils. Edmonton: The University of Alberta.
47. Vesic, A.S. (1961). “Beam on elastic subgrade and the Winkler hypothesis.” Proc., 5th Int. Conf. Soil Mech. and Found. Eng., Paris, France, Vol. 1, 845–850.
48. Yang Z, Lu J, Elgamal A (2008) OpenSees soil models and solid-fluid fully coupled elements User's Manual Ver 1:27.
49. Zhang, D.J.Y. 1999. Predicting capacity of helical screw piles in Alberta soils. M.E.Sc. Thesis, University of Alberta, Edmonton, Alberta, Canada.